anatomia

MDPI

Article

Vasculature of the Anterior Abdominal Wall and Surface Anatomy of the Liver and Stomach: Considerations for Minimal Access Surgeries in Neonates

Daniël J. van Tonder [1,2,*], Natalie Keough [2,3], Martin L. van Niekerk [4] and Albert van Schoor [2]

[1] Department of Basic Sciences, College of Medicine, Roseman University of Health Sciences, Las Vegas, NV 89135, USA
[2] Department of Anatomy, Faculty of Health Sciences, University of Pretoria, Pretoria 0001, South Africa; natalie.keough@warwick.ac.uk (N.K.); albert.vanschoor@up.ac.za (A.v.S.)
[3] Warwick Applied Health, Clinical Anatomy and Imaging, Warwick Medical School, University of Warwick, Coventry CV4 7AL, UK
[4] Department of Paediatric Surgery, Faculty of Health Sciences, University of Pretoria, Pretoria 0001, South Africa; admin@drmlvanniekerk.co.za
* Correspondence: dvantonder@roseman.edu

Abstract

Background: Minimal access surgeries are growing more common in neonatal care, but the risk of accidental injury to abdominal wall blood vessels remains a concern. This risk is increased by limited precise anatomical data specific to neonates. Therefore, this study aimed to quantitatively map the superficial and deep blood vessels of the neonatal anterior abdominal wall concerning important surgical landmarks to develop evidence-based recommendations for safer laparoscopic port placement. **Methods**: Thirty formalin-fixed low-birth-weight neonatal body donations ($\leq$4 weeks old) were dissected. An anatomical grid based on palpable landmarks—including the umbilicus, xiphoid process, and anterior superior iliac spines—was utilised to measure distances to the nearest vessels via digital image analysis. In situ topography of the liver, stomach, and umbilical vessels was also documented. **Results**: A midline corridor of reduced vascular density was identified; minimum circumferential distances to deep vessels above the umbilicus averaged 6.84–6.88 mm. Conversely, lateral regions were highly vascular, particularly at or below the transumbilical plane, with distances to deep vessels as short as 1.08 $\pm$ 0.83 mm. The liver and stomach extended significantly below the costal margin (averaging 20.61 $\pm$ 8.29 mm and 34.18 $\pm$ 14.44 mm, respectively). **Conclusions**: The results establish an anatomical foundation for using the reduced vascular midline for port placement and highlight the importance of inserting secondary lateral ports under direct visualisation.

Keywords: laparoscopy; abdominal wall; blood supply; epigastric arteries; anatomy

Check for updates

Academic Editor: Mugurel Constantin Rusu

Received: 31 January 2026
Revised: 14 April 2026
Accepted: 14 April 2026
Published: 21 April 2026

Copyright: © 2026 by the authors. Licensee MDPI, Basel, Switzerland. This article is an open access article distributed under the terms and conditions of the Creative Commons Attribution (CC BY) license.

1. Introduction

Minimal access surgeries, such as laparoscopic procedures, have gained favour among surgeons for procedures like appendicectomy, fundoplication, and hernia repair, offering well-documented benefits over traditional open surgical approaches [1,2]. The adoption of laparoscopic surgeries in the paediatric and, more specifically, the neonatal population has been a gradual but impactful process. The technology and instrumentation used during neonatal laparoscopy have advanced; however, procedures still require an experienced surgeon with specialised instruments [3] and a sound knowledge of the anatomy to

avoid iatrogenic injury to organs and vascular structures within the congested neonatal abdominal cavity.

1.1. Anatomical Background

Most of the arterial blood supply to the anterior abdominal wall comes from the superior, inferior, and superficial epigastric arteries, along with the intercostal arteries and the deep and superficial circumflex arteries [4]. The superior epigastric artery (TA2: arteria epigastrica superior), a terminal branch of the internal thoracic artery (TA2: arteria thoracica interna), descends posterior to the rectus abdominis muscle (TA2: musculus rectus abdominis). It eventually anastomoses with the inferior epigastric artery (TA2: arteria epigastrica inferior), which originates from the external iliac artery (TA2: arteria iliaca externa) [4]. Numerous perforators pass through the rectus abdominis muscles, providing blood supply to the overlying skin [5]. The superficial epigastric artery (TA2: arteria epigastrica superficialis) originates from the femoral artery, courses subcutaneously, and supplies the superficial anterior abdominal wall [4]. While the macroscopic course of these vessels is well-documented in adults [6–9], the topography of these vessels in the peadiatric abdomen remains under-reported. Awareness of vascular topography could help clinicians avoid vascular trauma during percutaneous instrumentation.

1.2. Surgical Approach

Insufflation of carbon dioxide (CO_2) gas through the Veress needle helps maintain a pneumoperitoneum before the insertion of the first trocar [2]. The umbilicus is the most common insertion site; however, Holcomb and Rothenberg [2] strongly recommend that in patients younger than 2 months, an infraumbilical ring approach be used. Inserting a Veress needle or trocar directly into this region carries the risk of creating a direct path for CO_2 gas to enter the systemic circulation. This can lead to a CO_2 embolism, a rare but potentially serious complication that can result in significant neurological impairment or death [2]. Once sufficient insufflation of the peritoneal cavity has been achieved, selection of entry sites for the camera and working instruments is a primary determinant of surgical success, impacting operative time, the surgeon's ability to manoeuvre instruments, and the overall safety of the procedure. Suboptimal port placement can transform a routine operation into a technically challenging endeavour, limiting visualisation and restricting the range of motion necessary for precise dissection and suturing. Transillumination has been suggested as an additional technique to improve safety, as it identifies epigastric vessels by shining a light from the laparoscope through the abdominal wall, allowing the surgeon to choose a port insertion site that avoids the epigastric vessels, thereby reducing the risk of port-site hematomas [10]. However, the effectiveness of transillumination is limited. It is less effective at identifying deeper vessels, and its utility decreases with increasing patient BMI, as light cannot penetrate adipose tissue sufficiently [10]. To avoid injury to the inferior epigastric vessels, direct laparoscopic visualisation from the abdominal cavity is recommended [11].

Despite the numerous minimally invasive surgeries being performed, and with the development of laparoscopic surgeries being refined since 1970 [3], studies have successfully shown that ultrasound can be used to identify vasculature within a neonatal population [12]. However, these studies focus on small areas, from established anatomical landmarks, and lack the ability to visualise the entire course of the vessels, unlike the dissection of the vessel throughout its course. Currently, there is little to no anatomical data that quantitatively evaluates the vasculature of the neonatal anterior abdominal wall in relation to reliable surgical landmarks. Therefore, this study aimed to quantitatively demonstrate the location of the superficial and deep vasculature of the neonatal anterior abdominal wall, including

the umbilical arteries and vein, through formalin-fixed whole-body donation dissection. It also aimed to define the position of the liver and stomach relative to the anterior abdominal wall, to elaborate on evidence-based guidelines for optimal laparoscopic trocar port placement, considering procedures both superior and inferior to the umbilicus.

2. Materials and Methods

The sample consisted of 30 formalin-fixed neonatal whole-body donations (also referred to as cadavers) of very low (<1.5 kg) to low birth weight (<2.5 kg), all of whom were four weeks old or less at the time of death. All the cadavers were donated to the Department of Anatomy at the University of Pretoria for research and teaching purposes through the body donation programme of the National Tissue Bank in Pretoria. The study adhered to the National Health Act of 2003, the Declaration of Helsinki (2024), and did not collect any identifiable information (Ethics Reference No: 224/2023). Neonatal cadavers with any developmental abnormalities of the thorax, abdomen, inguinal region, lower extremities, or any previous dissections that disrupted the normal anatomy of these regions were excluded. Sex and ancestry were not considered as exclusion factors.

2.1. Dissection Procedure for the Superficial Vascular Structures

Using Fisherbrand™ microdissection tools (Thermo Fisher Scientific, Waltham, MA, USA), a midline skin incision was made extending from the xiphisternal joint to the pubic symphysis. This was followed by two additional skin incisions, both on the left and right sides, which follow the costal margins to the midaxillary line. These incisions were then extended towards the thigh and terminated near the inguinal fold (Figure 1A,B). The skin was then carefully reflected inferiorly to expose the underlying superficial vascular structures (Figure 1C).

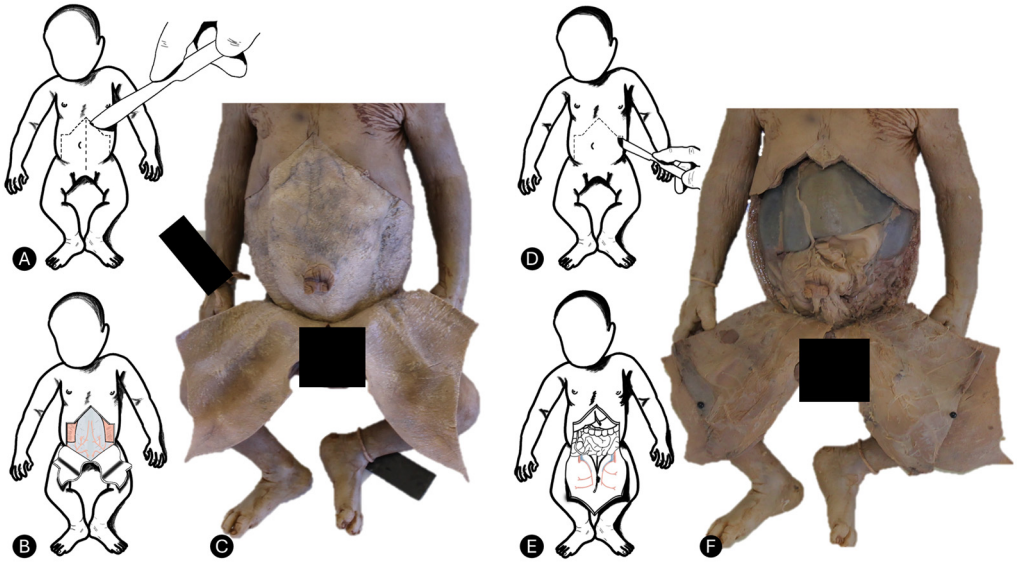


Figure 1. Schematic and visual representation of the incision made during dissection. (**A**) Schematic representation of the superficial skin incision made into the abdomen. (**B**) Schematic representation of skin folds reflected inferiorly to allow the identification of the superficial vascular structure. (**C**) Skin flaps of the anterior abdominal wall reflected inferiorly, to reveal the underlying fat, fascia, and superficial vasculature. (**D**) Deep skin incision through the anterior abdominal wall. (**E**) Schematic representation of the skin and rectus sheath reflected inferiorly, revealing the deep vascular structures. (**F**) The anterior abdominal wall reflected inferiorly, depicting the deep vasculature of the anterior abdominal wall, as well as the peritoneal cavity and anatomical structures within.

Using blunt dissection, the fat and fascia overlying the superficial vascular structures were carefully removed until the vascular structures were clearly visible. After all the required structures had been identified, the anatomical planes and landmarks were marked, as detailed in Figure 2A. Photos of the dissected area were captured using a Sony A1 Mirrorless Camera (Sony©, 2022, Nihonbashi, Tokyo, Japan) with a f1.1 50× camera lens (Sony©, 2022, Nihonbashi, Tokyo, Japan) set at a standard height using a tripod, with a scale next to and at the level of the dissected area. This enabled the anatomical grid to be determined using Fiji (ImageJ version 1.54p, Java 1.8.0_322; http://imagej.org) [13] photo-processing software. Each photograph was calibrated with the in-frame metric scale to minimise measurement errors caused by slight variations in tripod height, camera angle, or focal depth during different dissections. Once the anatomical grid was established, each identifiable superficial vascular structure was then followed from its origin to its termination and identification markers were placed, using Fiji, at each location where the vascular structure bisects an anatomical plane. Measurements were then taken from each major anatomical point, determined by intersecting planes or a predetermined anatomical landmark (Figure 2A).

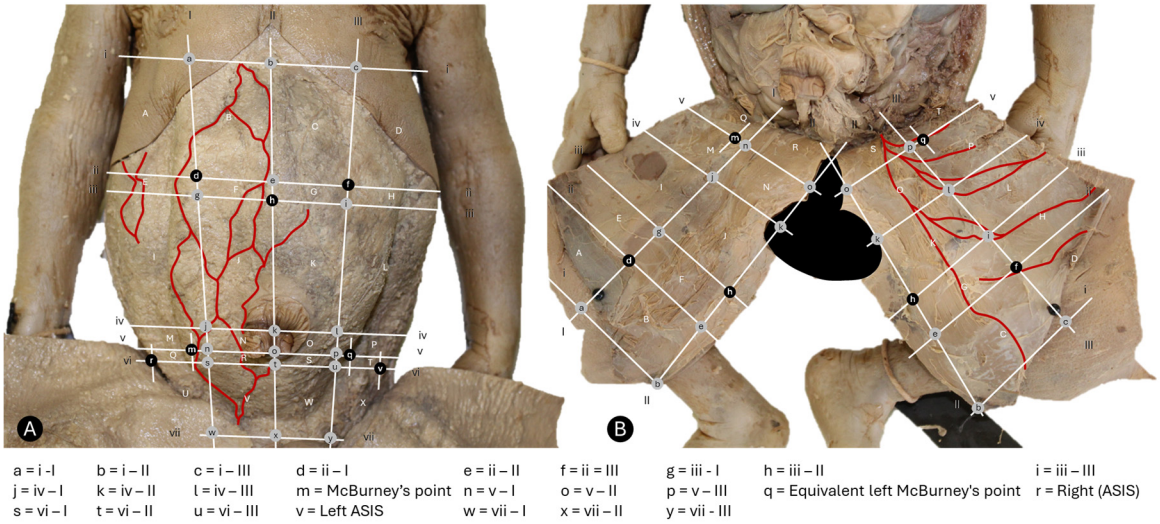


Figure 2. An anatomical grid established to measure (**A**) superficial vascular structures and (**B**) the deep vasculature of the anterior abdominal wall. (I) Line through the right midclavicular line and the right mid-inguinal line. (II) Mid-sagittal line—line through the xiphisternal joint, Lee-Huang's point and pubic symphysis. (III) Line through the left midclavicular line and the left mid-inguinal line. (i) Transverse line through the xiphoid process. (ii) Subcostal plane. (iii) Transverse line through Lee-Huang's point. (iv) Transumbilical plane. (v) Transverse line McBurney's points. (vi) Line through both anterior superior iliac spine (ASIS)—ASIS axes. (vii) Line through the superior surface of the pubic crests.

From each of the anatomical points, determined by intersecting planes or predetermined anatomical landmarks (Figure 2A), a measurement in each direction, i.e., superior, medial, inferior, and lateral, as well as minimal circumferential distance (irrespective of direction), was recorded to the closest vasculature structure. For anatomical points within the midline (median), a superior, left, inferior, and right, including a minimal circumferential measurement, were taken.

2.2. Dissection Procedure for the Deep Vascular Structures

To determine the deep vascular structures of the abdomen, a deep incision was made into the abdominal cavity through the external oblique, internal oblique, and transverse abdominis muscles. Starting at the xiphoid process, the incision was continued to both

the left and right midaxillary lines following the costal margin. These incisions were extended into the thigh towards the inguinal fold (Figure 1D,E). An additional incision was made down the midline, around the umbilicus, to the pubic symphysis. The anterior abdominal wall was then carefully reflected inferiorly to expose the deep vascular structures (Figure 1F). Great care was taken to reflect both the right and left sides to reveal the deep vascular structures of the anterior abdominal wall, including the inferior epigastric arteries, the umbilical arteries and the umbilical vein. The falciform ligament of the liver was also dissected as close as possible to the liver.

Using blunt dissection, the fat and fascia overlying the deep vascular structures were removed. The anatomical points were marked (Figure 2B) using Fiji photo processing software, and the measurements in each direction, i.e., lateral, medial, superior, and inferior, as well as the minimal circumferential distance (irrespective of direction), were recorded to the closest vasculature structure. For measurements within the midline (median), a superior, left, inferior, and right, including a minimal circumferential measurement, were taken.

To locate the in situ positions of the inferior epigastric arteries, the umbilical arteries and the umbilical vein, and to determine the surface anatomy of the liver and stomach, an image of the dissected abdominal cavity was taken with a scale at the dissection site. This allowed for the establishment of the anatomical grid using Fiji photo-processing software. Measurements were then made from each key anatomical point to the closest vascular structure. Additionally, the distances from the subcostal margin to the lower edge of the liver and stomach along the right and left midclavicular lines and the mid-sagittal plane were recorded. The frequency with which the liver or stomach was entirely, partially, or not in an anatomical cell (A–X) was then documented.

2.3. Statistical Analyses

Using IBM SPSS Statistics for Windows, version 29.0.2.0 (IBM Corp., Armonk, NY, USA), the datasets were analysed to determine the metric variables of the mean ± standard deviation (SD), median, minimum, maximum, and ranges, as well as a 95% confidence interval (CI). Frequency was used as a descriptive statistic for the ordinal variables. To reduce recording errors and extreme biological measurements that would skew the mean and standard deviation, a total of 48 directional measurements, representing less than 0.86% (n = 5606) of the total comprehensive dataset, yielded Z-scores that were greater than 3 or less than −3 and were removed from the dataset. This was to ensure the quantitative results accurately represented the typical structural and vascular patterns of the low-birth-weight neonatal anterior abdominal wall. This anatomical framework allows for the description of vascular density across the abdominal wall. However, pooling measurements from different directions within a single specimen introduces some statistical dependence. This means that neonatal specimens with complex or dense vascular branching may slightly skew the average measurements in certain local quadrants. Nonetheless, this clustering is a natural consequence of topographical mapping and does not compromise the overall conclusions.

To visualise the data, kernel density plots, which are continuous estimates of the probability density function of a continuous random variable [14], were generated by transforming each measurement to a proportional value (zero to one) based on each individual measurement in proportion to the distance from one plane to the next. As such, within Figure 3, the x-axis presents the standardised measurements, ranging from 0 (the lowest original value) to 1 (the highest original value). The y-axis (height of the curves) indicates the concentration of data points at a specific standardised value. A high peak (or wider section of the curve) means that many measurements across the entire dataset fall close to that standardised value. A low point, or a flattened curve, means that very few measurements fall in that range. These density plots should be

interpreted as visual representations of spatial trends rather than precise predictors of vascular location or surgical risk. It should be noted that each specimen contributed multiple directional measurements across predefined anatomical landmarks. The unit of analysis was therefore the individual measurement at each anatomical point. While some degree of within-specimen correlation is inherent in this design, the analysis was conducted within a descriptive anatomical framework, where each measurement represents a distinct spatial relationship within the grid. As such, measurements were pooled to characterise overall anatomical patterns, and clustering effects were not formally modelled. The findings should therefore be interpreted as descriptive of anatomical trends rather than as statistically independent observations. From the sample size of 30, more than 10% of the sample (n = 5) was re-examined by the co-author and the principal investigator to determine inter- and intra-observer error, respectively. An analysis to test the repeatability and accuracy of the data was conducted using a Bland–Altman plot for assessing the agreement between two quantitative measurement methods [15].

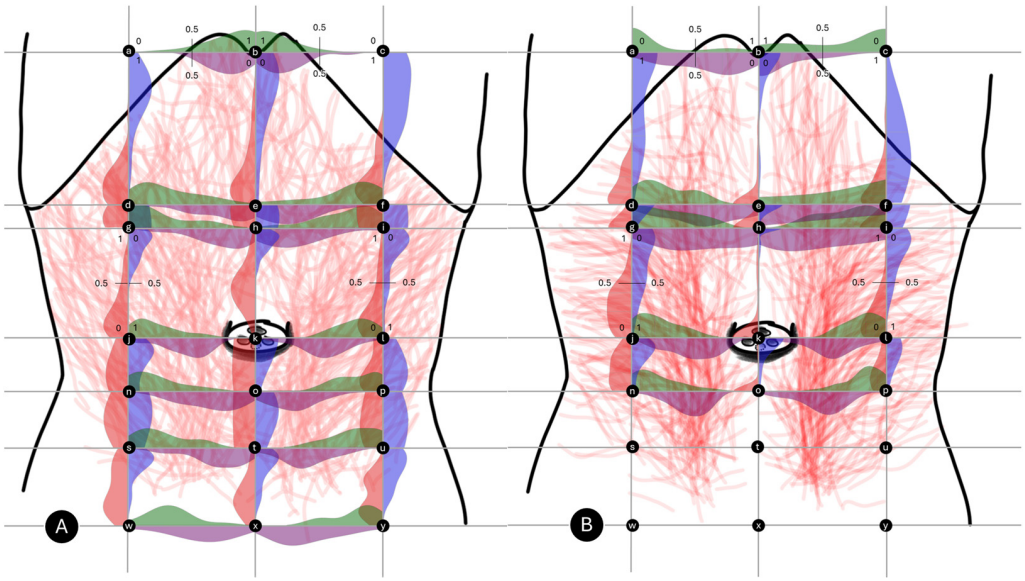


Figure 3. Visual representation of the vasculature structures of the (**A**) superficial anterior abdominal wall and (**B**) deep anterior abdominal wall. Vasculature was traced after individual dissections were morphed to the anatomical grid and overlapped. Overlayed are kernel density plots showing the standardised distribution of the intersections between vascular structures and the respective planes. The height of the curves indicates the concentration of data points at a specific standardised value. GREEN indicates medial measurements, PURPLE shows left and right, BLUE denotes inferior measurements, and RED highlights superior measurements between indicated anatomical landmarks.

3. Results

The mean age of the sample was 1.77 ± 5.46 days (mean ± SD). The mean height and weight of the sample were 38.17 ± 6.87 cm and 1.77 ± 1.16 kg, respectively. The sample comprised 33.3% (n = 10) females and 66.7% (n = 20) males, with an ancestry distribution of 86.7% (n = 26) South African Black and 13.3% (n = 4) South African White individuals.

3.1. Superficial Vascular Structures of the Anterior Abdominal Wall

Within the established anatomical grid, the superior, medial, inferior, and lateral measurements at each established anatomical landmark (superior, left, inferior, and right measurements were obtained for anatomical landmarks in the midline) are summarised in Tables 1–3, and visualised in Figure 3A. Figure 3 show the standardised measurements (measurement from the anatomical point to the closest vasculature divided by total distance

between anatomical points) at the anatomical points in each direction relative to the closest vasculature structure.

On average, the anatomical landmark points "k", "w", "x", and "y" demonstrated the greatest minimal circumferential (in no specific direction) distances of 5.80 ± 2.66 mm, 4.78 ± 2.97 mm, 5.47 ± 3.87 mm, and 4.10 ± 3.10 mm, respectively, outside of the pathway of underlying abdominal vascular structures. This is also seen in Figure 3A, with peaks around these points that are further away from the anatomical points mentioned above.

3.1.1. Above the Level of the Umbilicus

Superior to the transumbilical plane, transverse lines through the xiphoid process and Lee-Huang's point, together with the subcostal plane, established intersections with the right midclavicular line (anatomical landmark points "a", "d", and "g"), the mid-sagittal plane (anatomical points "b", "e", and "h"), and left midclavicular plane (anatomical landmark points "c", "f", and "i"). Points "a" and "c" had no superior and lateral values, as this extended outside of the dissection area, and no observations were made in those two directions.

Right Midclavicular Line: Anatomical Landmark Points "a", "d", and "g"

The pathways of the superficial vascular structures of the anterior abdominal wall were found on average (closest distance) between 2.62 and 3.45 mm above these landmark points in the right midclavicular line, 3.15–15.58 mm inferior to these landmark points, 4.10–15.61 mm medial to these landmark points, and 3.37–4.25 mm lateral to these anatomical landmark points (Table 1). Although the kernel density plot peaks (Figure 3A) are further away from the anatomical point "a", it bears considering that some of those points (superior and lateral) are above the costal margin, and extended outside the dissection area; thus, closer vasculature was not recorded.

Table 1. Closest mean distance (in mm) from anatomical landmarks to the nearest superficial vasculature in two perpendicular planes; four directional measurements taken above the level of the umbilicus. (Sup = Superior, Med = Medial, Inf = Inferior, Lat = Lateral, SD = Standard deviation.)

	Directional Measurement at Each Anatomical Landmark											
	Sup	**Med**	**Inf**	**Lat**	**Sup**	**Left**	**Inf**	**Right**	**Sup**	**Med**	**Inf**	**Lat**
		a				**b (Xiphoid process)**				**c**		
N		26	27		11	25	29	25		26	26	
Range		25.28	22.62		6.22	8.98	20.65	7.81		19.97	19.84	
Mean		15.61	15.58		3.56	3.88	6.41	3.84		16.86	16.21	
SD		5.74	6.50		2.04	2.46	5.96	2.44		4.98	5.64	
		d				**e**				**f**		
N	26	27	28	25	26	28	29	29	22	29	27	26
Range	10.61	12.64	12.32	11.52	11.00	17.01	9.80	11.86	12.80	14.24	10.33	10.66
Mean	3.45	4.44	5.24	4.25	3.42	5.26	3.68	4.11	3.81	4.58	3.19	3.76
SD	2.67	3.24	3.79	2.95	3.05	4.58	2.77	3.51	3.52	3.80	2.95	3.54
		g				**h (Lee-Huang's Point)**				**i**		
N	28	29	28	27	27	27	27	28	27	30	29	28
Range	9.32	14.76	9.90	9.63	13.86	14.93	8.60	10.13	14.30	17.31	15.93	14.46
Mean	2.62	4.10	3.15	3.37	4.42	5.04	2.97	4.22	4.26	4.81	4.44	4.07
SD	2.38	4.01	2.69	2.78	3.60	3.87	2.37	2.91	3.90	3.58	4.80	3.46

Mid-Sagittal Plane: Anatomical Landmark Points "b", "e", and "h"

The course of superficial vascular structures of the anterior abdominal wall was found on average (closest distance) between 3.42 and 4.42 mm superiorly, 2.97–6.41 mm inferiorly, 3.88–5.26 mm to the left, and 3.84–4.22 mm to the right of these anatomical landmark points in the mid-sagittal plane (Table 1). Considering the kernel density plots (Figure 3A), there is a significant accumulation of high peaks surrounding point "b", with GREEN indicating medial measurements from points "a" and "c" and PURPLE indicating the left and right distances from point "b". This indicates that the left and right measurements from point "b" (xiphoid process) were consistently similar, possibly the same, as the superficial vasculature measured from anatomical landmark points "a", "b", and "c". When taking into account all three anatomical points ("b", "e", and "h"), and the density distribution found to the left and right, a general trend is noted that the superficial vasculature courses laterally to the midline, as they course cranially.

Left Midclavicular Line: Anatomical Landmark Points "c", "f", and "i"

When considering the course of the superficial vascular structures of the anterior abdominal wall in this plane, the average closest distance was found between 3.81 and 4.26 mm superior to these landmark points in the left midclavicular line, 3.19–16.21 mm inferior to these landmark points, 4.58–16.86 mm medial to these landmark points, and 3.76–4.07 mm lateral to these landmark points (Table 1). Similar to anatomical point "a", point "c" is above the costal margin, and a point closer to the vasculature might be present; however, this extends outside of the dissection area. When considering the kernel density plots (Figure 3A) surrounding points "f" and "i", the superior (RED) and inferior (BLUE) plots indicate a higher frequency that vasculature is found near those anatomical points. The vasculature found medially is more equally distributed away from the anatomical points; however, it still presents with a high frequency of the vasculature crossing the plane closer to the anatomical point.

3.1.2. At the Level of the Umbilicus

Three intersections with the transumbilical plane were recorded as anatomical landmarks in Table 2: one at the right midclavicular line ("j"), another in the mid-sagittal plane ("k"), and the last at the left midclavicular line ("l").

Table 2. Closest mean distance (in mm) from anatomical landmarks to the nearest superficial vasculature in two perpendicular planes; four directional measurements taken at the level of the umbilicus. (Sup = Superior, Med = Medial, Inf = Inferior, Lat = Lateral, SD = Standard deviation.)

	Directional Measurement at Each Anatomical Landmark											
	Sup	**Med**	**Inf**	**Lat**	**Sup**	**Left**	**Inf**	**Right**	**Sup**	**Med**	**Inf**	**Lat**
	j				**k (Umbilicus)**				**l**			
N	29	30	30	27	27	30	27	29	30	30	29	29
Range	18.79	12.90	10.16	12.88	17.59	14.64	11.01	12.67	18.64	9.67	13.76	12.13
Mean	5.51	3.54	3.45	4.15	11.20	9.31	7.80	9.71	4.88	3.68	4.28	4.83
SD	5.19	3.07	2.83	3.50	4.32	3.69	2.84	3.41	4.63	2.37	3.28	3.50

Anatomical Landmark Points "j", "k", and "l"

Point "j" revealed that, on average, a vessel was found 5.51 ± 5.19 mm superiorly, 3.54 ± 3.07 mm medially, 3.45 ± 2.83 mm inferiorly, and 4.15 ± 3.50 mm laterally. Similar values were seen for point "l", as on average the closest vasculature found superiorly was 4.88 ± 4.63 mm, 3.68 ± 2.37 mm medially, 4.28 ± 3.28 mm inferiorly, and 4.83 ± 3.50 mm

laterally. In reference to Figure 3A, the anatomical points "j" and "l" have high peaks surrounding the point, indicating that the vasculature is near the determined intersections. This is unlike point "k," which shows a barren region near the anatomical point, with the highest density peak of the vasculature crossing the plane to the left, right, and superiorly, roughly halfway between the adjacent anatomical points. However, the kernel density plot for the vasculature inferior to point "k" indicates a general distribution, with no prominent high-density peaks. On average, the closest superficial vasculature found from point "k", circumferential, was 5.80 ± 2.66 mm (95% CI: 4.81–6.79 mm). The average distance from point "k" to the closest vasculature superiorly was 11.20 ± 4.32 mm, 9.31 ± 3.69 mm to the left, 9.71 ± 3.41 mm to the right, and 7.80 ± 2.84 mm inferiorly.

3.1.3. Below the Level of the Umbilicus

Just inferior to the transumbilical plane, transverse lines through the McBurney's point, ASIS, and the palpable pubic crests were established, intersecting with the right midclavicular line, anatomical landmark points "n", "s", and "w", the mid-sagittal plane, anatomical points "o", "t", and "x", and left midclavicular plane, anatomical landmark points "p", "u", and "y" (Table 3). In addition to anatomical landmarks within the established grid, four additional distinct anatomical landmarks were identified. These included one at McBurney's point (right side), point "m", another at the contralateral equivalent of McBurney's point (left side), point "q", and the right (point "r") and left (point "v") ASIS. At each of these landmarks, two perpendicular planes were established, one parallel to the midclavicular lines and the other to the transverse plane, facilitating four measurements—superior, medial, inferior, and lateral—at each of the four locations.

Table 3. Closest mean distance (in mm) from anatomical landmarks to the nearest superficial vasculature in two perpendicular planes; four directional measurements taken below the level of the umbilicus. (Sup = Superior, Med = Medial, Inf = Inferior, Lat = Lateral, SD = Standard deviation.)

	Directional Measurement at Each Anatomical Landmark											
	Sup	**Med**	**Inf**	**Lat**	**Sup**	**Left**	**Inf**	**Right**	**Sup**	**Med**	**Inf**	**Lat**
	n				**o**				**p**			
N	29	29	27	29	28	30	23	30	29	30	29	29
Range	19.20	11.69	7.54	12.25	34.02	14.16	4.86	13.62	10.48	9.47	14.37	11.90
Mean	4.44	3.34	2.32	3.45	10.92	5.45	2.02	6.11	3.18	3.52	4.02	4.49
SD	5.10	3.17	2.30	3.54	9.69	3.47	1.29	3.73	3.22	3.15	3.80	4.16
	s				**t**				**u**			
N	28	30	25	25	26	28	25	29	30	30	30	27
Range	5.85	14.15	5.95	11.33	22.02	14.25	18.37	15.45	9.83	13.47	11.80	8.93
Mean	3.01	4.75	2.50	3.57	5.55	6.36	4.44	5.35	2.97	3.77	4.44	4.01
SD	1.81	3.79	1.72	2.75	6.16	3.09	4.69	3.93	2.52	3.65	3.66	3.17
	w				**x (Pubic crests)**				**y**			
N	30	11	2	6	27	11	4	9	30	11	4	6
Range	18.60	11.26	1.47	5.51	16.12	14.62	6.05	14.49	18.74	9.36	1.72	6.68
Mean	7.86	5.39	0.73	2.39	7.25	7.21	2.77	7.24	6.28	3.49	1.71	3.72
SD	5.19	3.12	1.04	1.97	4.77	5.28	2.70	4.88	4.33	3.11	0.91	2.30

Right Midclavicular Line: Anatomical Landmark Points "n", "s", and "w"

Vascular structures of the anterior abdominal wall were found on average (closest distance) between 3.01 and 7.86 mm superior to these landmark points in the right midclavicular line, 0.73–2.50 mm inferior to these landmark points, 3.34–5.39 mm medial to these landmark points, and 2.39–3.57 mm lateral to these anatomical landmark points (Table 3). Considering the kernel density plots (Figure 3A) medial to the anatomical points within the right midclavicular line, the high-density peaks laterally migrate from the median as the vasculature coursed cranially. Point "w" has a density peak that is further medially than those of points "s" and "n". On average, the closest vasculature (circumferential) to point "w" was 4.78 ± 2.97 mm; medially, the closest vasculature was 5.39 ± 3.12 mm. Superior to point "w", the vasculature was seen on average, at the closest distance, at 7.86 ± 5.19 mm.

Mid-Sagittal Plane: Anatomical Landmark Points "o", "t", and "x"

On average, the closest distance from the anatomical points to the vascular structures of the anterior abdominal wall were between 10.92 and 5.55 mm superior, 4.44–2.02 mm inferior, 5.45–7.21 mm left, and 5.35–7.24 mm right to these anatomical landmark points in the mid-sagittal plane (Table 3).

Left Midclavicular Line: Anatomical Landmark Points "p", "u", and "y"

On the anterior abdominal wall, the superficial vasculature in relation to the left midclavicular line was on average between 2.97 and 6.28 mm superior, 1.71–4.44 mm inferior, 3.49–3.77 mm medial, and 3.72–4.49 mm lateral to these anatomical landmark points (Table 3). Considering the kernel density plots (Figure 3A) medial to the anatomical points within the left midclavicular line, the high-density peaks laterally migrate from the median as the vasculature coursed cranially, similar to the right side. The medial density plots at points "y" and "p" both have two high-density peaks, a bimodal distribution, suggesting that the vasculature bisected the plane at those levels at two separate common distances.

Planes Through McBurney's Point and the Contralateral Equivalent Anatomical Landmark Points "m" and "q"

The minimal circumferential distance from point "m" was 1.15 ± 0.079 mm (95% CI: 0.84–1.46 mm). Point "q" had similar results, with 3.84 ± 4.00 mm superiorly, 4.14 ± 3.86 mm medially, 2.68 ± 2.76 mm inferiorly, 3.36 ± 2.74 mm laterally, and an average minimal circumferential distance to the closest vasculature structure of 1.30 ± 1.30 (95% CI: 0.81–1.79 mm).

Planes Through ASIS: Anatomical Landmark Points "r" and "v"

The four directional measurements for the two anatomical landmarks associated with the right ("r") and left ("v") ASIS were measured superiorly ("r": 6.58 ± 4.19 mm, "v": 4.51 ± 2.74 mm), medially ("r": 5.71 ± 3.13 mm, "v": 4.76 ± 3.36 mm), inferiorly ("r": 4.35 ± 2.80 mm, "v": 3.17 ± 1.87 mm), laterally ("r": 3.40 ± 2.76 mm, "v": 2.25 ± 1.53 mm), and the to the minimal circumferential distance ("r": 2.73 ± 2.02 mm; 95% CI:1.98–3.48 mm, "v": 2.29 ± 2.03 mm; 95% CI: 1.50–3.08 mm) between the anatomical landmark and the vascular structure.

3.2. Deep Vascular Structures of the Anterior Abdominal Wall

Using the same established anatomical grid and superior, medial, inferior, and lateral measurements at each established anatomical landmark (superior, left, inferior, and right measurements at landmarks in the midline), the results are summarised in Tables 4–6, and visualised in Figure 3B.

3.2.1. Above the Level of the Umbilicus

The results from established intersections with the right midclavicular line, anatomical landmark points "a", "d", and "g", the mid-sagittal plane, anatomical points "b", "e", and "h", and the left midclavicular plane, anatomical landmark points "c", "f", and "i", are shown in Table 4. Points "a" and "c" had no superior and lateral values, as this extended outside of the dissection area, and no observations were made in those two directions.

Table 4. Closest mean distance (in mm) from anatomical landmarks to the nearest vasculature in two perpendicular planes; four directional measurements taken above the level of the umbilicus. (Sup = Superior, Med = Medial, Inf = Inferior, Lat = Lateral, SD = Standard deviation.)

Directional Measurement at Each Anatomical Landmark												
	Sup	**Med**	**Inf**	**Lat**	**Sup**	**Left**	**Inf**	**Right**	**Sup**	**Med**	**Inf**	**Lat**
			a				**b (Xiphoid process)**				**c**	
N	0	5	13	0	0	12	7	6	0	11	13	0
Range		11.63	11.91			12.79	19.8	11.17		14.29	20.79	
Mean		11.86	15.53			8.41	12.07	6.57		16.61	19.76	
SD		4.22	4.13			4.39	7.73	4.43		5.39	6.30	
			d				**e**				**f**	
N	22	28	30	24	5	29	5	29	22	28	28	17
Range	17.85	11.12	18.68	16.49	17.66	22.35	5.24	21.12	10.8	14.35	15.66	19.93
Mean	4.80	4.68	5.35	4.62	7.66	11.41	3.41	8.45	4.05	4.98	6.50	5.51
SD	4.17	3.52	4.48	4.20	6.77	5.71	2.16	5.61	3.21	4.21	4.92	5.03
			g				**h (Lee-Huang's Point)**				**i**	
N	12	24	28	10	7	28	6	27	7	29	27	13
Range	10.79	10.27	16.79	10.11	17.26	22.59	7.24	21.94	11.7	22.08	18.13	8.9
Mean	6.93	5.82	6.75	3.30	6.10	9.68	3.08	9.99	4.13	6.63	5.69	5.31
SD	3.31	3.35	5.24	3.58	5.90	6.18	2.74	6.36	4.53	5.45	4.89	2.42

Right Midclavicular Line: Anatomical Landmark Points "a", "d", and "g"

The minimal distance from "a" in a medial and inferior direction was 11.86 ± 4.22 mm and 15.53 ±4.13 mm, respectively (Table 4). The kernel density plots (Figure 3B) around point "a" present relatively flat plots in all directions, indicative that there was no common site where the vasculature bisected the planes. The minimum circumferential distance from the anatomical landmarks to a vascular structure that was the closest to the points was "d" (2.37 ± 2.23 mm; 95% CI: 1.55–3.19 mm) and "g" (4.03 ± 3.26 mm; 95% CI: 2.79–5.27 mm).

Mid-Sagittal Plane: Anatomical Landmark Points "b", "e", and "h"

The vasculature surrounding the median anatomical landmarks "e" and "h" on both sides are positioned relatively further away, compared to the anatomical points situated in the right and left midclavicular lines. On average, the closest distances (Table 4) to the left of these points were 8.41 ± 4.39 mm for "b", 11.41 ± 5.71 mm for "e", and 6.10 ± 5.90 mm for "h". To the right, the average closest distances were 6.57 ± 4.43 mm for "b", 8.45 ± 5.61 mm for "e", and 9.99 ± 6.36 mm for "h". This vacant vasculature corridor is apparent in Figure 4, with some discrepancy around points "e" and "h", which shows a flat distribution from the point. The flat distribution is confirmed with the SD ranging between 5.71 mm and 5.61 mm for left and right measurements from point "e", and 9.68 and 9.99 mm for the measurements to the left and right of point "h". On average, the minimum circumferential distance from anatomical landmarks to a vascular structure that was further away was at point "b"

(8.78 ± 4.87 mm; 95% CI: 6.90–10.67 mm), "e" (6.84 ± 4.44 mm; 95% CI: 5.21–8.47 mm), and "h" (6.88 ± 5.76 mm; 95% CI: 4.73–9.03 mm), compared to the average distance within the right and left midclavicular lines.

Left Midclavicular Line: Anatomical Landmark Points "c", "f", and "i"

The shortest medial distance from point "c" to the closest vasculature structure was 16.61 ± 5.39 mm, and inferiorly 19.76 ± 6.30 mm (Table 4). Meanwhile, the minimum circumferential distance from the anatomical landmarks points "f" and "i" was 2.76 ± 2.71 mm (95% CI: 1.77–3.75 mm) and 2.46 ± 2.29 mm (95% CI: 1.59–3.33 mm), respectively.

3.2.2. At the Level of the Umbilicus

Three intersections with the transumbilical plane were recorded at points "j", "k", and "l" (Table 5).

Table 5. Closest mean distance (in mm) from anatomical landmarks to the nearest vasculature in two perpendicular planes; four directional measurements taken at the level of the umbilicus. (Sup = Superior, Med = Medial, Inf = Inferior, Lat = Lateral, SD = Standard deviation.)

	Directional Measurement at Each Anatomical Landmark											
	Sup	**Med**	**Inf**	**Lat**	**Sup**	**Left**	**Inf**	**Right**	**Sup**	**Med**	**Inf**	**Lat**
	j				**k (Umbilicus)**				**l**			
N	31	31	30	30	3	31	5	31	29	29	28	24
Range	14.37	7.78	11.4	12.97	6.1	19.19	9.35	17.62	18.93	8.33	8.17	5.22
Mean	6.16	3.40	4.03	3.40	7.50	10.87	8.78	9.70	4.54	3.12	3.29	2.08
SD	4.48	2.42	3.16	3.22	3.09	4.40	3.50	5.03	4.97	2.41	2.75	1.73

Anatomical Landmark Points "j", "k", and "l"

At the umbilicus (point "k"), the nearest vascular structures were approximately 7.50 ± 5.90 mm above, 10.87 ± 4.40 mm to the left, 8.78 ± 3.50 mm below, and 3.08 ± 2.74 mm to the right (Table 5). The average minimum circumferential distance from point "k" to a vascular structure was 7.29 ± 4.08 mm (95% CI: 5.79–8.78 mm). The closest circumferential vascular structures to the points were near "j" at 1.08 ± 0.83 mm (95% CI: 0.77–1.39 mm) and to point "l" 1.45 ± 1.16 mm (95% CI: 1.02–1.88 mm). Figure 3B, specifically between points "k" and "h", depicts a region of reduced vasculature midway between the two anatomical landmark points. High-density peaks are visible near the two points, with very few instances of vasculature crossing between them farther away. Since the methodology only recorded the closest vasculature, there might be a third vasculature structure between the two points that is neither close to "h" nor "k" and may not have been recorded. The kernel density plots on either side of point "k" indicate that the majority of vasculature crossing the transumbilical plane would have been further away from point "k", approximately midway between points "j" and "l".

3.2.3. Below the Level of the Umbilicus

The deep abdominal wall dissection area limited the measurements to the points located on the horizontal line through McBurney's point. The anatomical landmark points "n", "o", and "p" are listed in Table 6, whereas the points "q", "r", "s", "t", "u", "v", "w", "x", and "y" have no comparable measurements.

Table 6. Closest mean distance (in mm) from anatomical landmarks to the nearest vasculature in two perpendicular planes; four directional measurements taken below the level of the umbilicus. (Sup = Superior, Med = Medial, Inf = Inferior, Lat = Lateral, SD = Standard deviation.)

	Directional Measurement at Each Anatomical Landmark											
	Sup	**Med**	**Inf**	**Lat**	**Sup**	**Left**	**Inf**	**Right**	**Sup**	**Med**	**Inf**	**Lat**
				n			**o**				**p**	
N	30	31	29	22	3	31	4	31	30	30	27	27
Range	17.02	10.06	10.87	12.49	6.81	17.56	2.71	11.86	14.36	9.26	6.24	12
Mean	5.71	3.41	4.22	3.14	5.06	9.49	4.17	9.90	4.81	3.10	1.87	3.24
SD	4.81	3.04	3.06	4.12	3.41	4.33	1.38	3.60	3.81	2.59	1.56	3.72

Right Midclavicular Line: Anatomical Landmark Point "n"

The minimum circumferential distance from the anatomical landmarks to a vascular structure that was the closest to the points was "n" (1.75 ± 1.76 mm; 95% CI: 1.11–2.40 mm).

Mid-sagittal Plane: Anatomical Landmark Point "o"

Below the umbilicus, where the horizontal line through McBurney's point intersects with the mid-sagittal plane, the nearest vascular structure to point "o" was, on average, 5.06 ± 3.41 mm above, 9.49 ± 4.33 mm to the left, 4.17 ± 1.38 mm below, and 9.90 ± 3.60 mm to the right (Table 6). On average, the minimum circumferential distance at point "o" was 6.66 ± 3.17 mm (95% CI: 5.49–7.82 mm). A vacant vasculature corridor is apparent within Figure 3B, as we visually note the high peaks further away from points "k" and "o".

Left Midclavicular Line: Anatomical Landmark Point "p"

The minimum circumferential distance from the anatomical landmarks point "p" to a vascular structure was 1.16 ± 1.27 mm (95% CI: 0.68–1.64 mm).

3.3. Internal Vasculature and Organs of the Abdominal Cavity

The umbilical vein was found in the midline at point "e". On twelve (n = 12) occasions, the umbilical veins were found to the right of point "e", with an average distance of 0.80 ± 0.88 mm, and on eleven (n = 11) occasions to the left of point "e", with an average distance of 0.59 ± 0.85 mm. The horizontal measurements of the in situ umbilical vein were on average 18.97 ± 5.26 mm medial to point "d", and 21.00 ± 4.94 mm medial to point "f". At the level of Lee-Huang's point (point "h"), the umbilical vein was found 17.38 ± 6.47 mm from the intersection with the right midclavicular line (point "g"), and on average was found 20.97 ± 6.39 mm from point "i", the intersection between Lee-Huang's point and the left midclavicular line.

Below the umbilicus, the average shortest horizontal distances to the umbilical arteries were 8.95 ± 2.86 mm medially from point "n" and 11.94 ± 3.42 mm medially from point "p". The average lateral measurements from point "o" to the right were 2.22 ± 2.53 mm, and to the left 2.14 ± 2.10 mm. More caudally, at the level of the ASIS (point "s"), the umbilical arteries were on average 6.96 ± 2.88 mm medially, and from point "u", the umbilical arteries were medially on average 9.44 ± 3.61 mm. From point "t", the umbilical arteries were on average 2.48 ± 2.21 mm to the right, and 3.89 ± 3.76 mm to the left. The minimal circumferential distances from point "t" were 2.22 ± 2.25 mm (95% CI: 1.33–3.11 mm).

In addition to determining the surface anatomy of the liver and stomach within specific anatomical cells (A–L), measurements of the distance from the subcostal border to the inferior margins of both organs were used to describe the surface anatomy. Table 7

summarises the frequency of liver and stomach in each anatomical cell; a visual representation of these values is also depicted in Figure 4. The liver was consistently observed in cells A–C. In cell A, the liver either completely occupied the entirety of the cell (93.5%), or only partially occupied some of the cell (6.5%). Similarly, in cell B, the liver was completely present 80.6% of the time and partially present in the remaining 19.4% of cases. In cell C, the liver was partially located in 54.8% of cases and only completely within the cell in 45.2% of cases. The liver was absent from cell D in 32.3% of cases and was found in varying degrees. In cell E, the liver was completely present in 83.9% of cases, partially in 9.7%, and absent in 6.5% of cases. The liver was only partially located or absent in cells I to L, with the frequency of its presence decreasing from right to left (I to L), from 83.9% to 25.8%. The inferior margin of the liver extended below the costal border on average by 17.34 ± 8.24 mm (95% CI: 14.26–20.42 mm) within the right midclavicular line, 20.61 ± 8.29 mm (95% CI: 17.56–23.65 mm) within the mid-sagittal plane, and 12.41 ± 8.32 mm (95% CI: 8.81–16.01 mm) within the left midclavicular line.

Table 7. Frequency table of the in situ location of the liver and stomach related to the established anatomical cells.

	Liver											
	Yes	**Partially**	**No**	**Yes**	**Partially**	**No**	**Yes**	**Partially**	**No**	**Yes**	**Partially**	**No**
		A			**B**			**C**			**D**	
Freq (n)	29	2	0	25	6	0	14	17	0	6	15	10
(%)	93.5	6.5	0	80.6	19.4	0	45.2	54.8	0	19.4	48.4	32.3
		E			**F**			**G**			**H**	
Freq (n)	26	3	2	17	10	4	8	13	10	3	10	18
(%)	83.9	9.7	6.5	54.8	32.3	12.9	25.8	41.9	32.3	9.7	32.3	58.1
		I			**J**			**K**			**L**	
Freq (n)	0	26	5	0	22	9	0	13	18	0	8	23
(%)	0	83.9	16.1	0	71	29	0	41.9	58.1	0	25.8	74.2
	Stomach											
	Yes	**Partially**	**No**	**Yes**	**Partially**	**No**	**Yes**	**Partially**	**No**	**Yes**	**Partially**	**No**
		A			**B**			**C**			**D**	
Freq (n)	0	1	28	0	1	28	0	12	17	0	17	12
(%)	0	3.4	96.6	0	3.4	96.6	0	41.4	58.6	0	58.6	41.4
		E			**F**			**G**			**H**	
Freq (n)	0	0	29	0	4	25	0	16	13	0	21	8
(%)	0	0	100	0	13.8	86.2	0	55.2	44.8	0	72.4	27.6
		I			**J**			**K**			**L**	
Freq (n)	0	1	28	0	5	24	0	12	17	0	14	15
(%)	0	3.4	96.6	0	17.2	82.8	0	41.4	58.6	0	48.3	51.7

The stomach was most frequently observed within the anatomical cell H. Within this sample, the stomach never completely occupied a single anatomical cell and was only partially visible in cell H 72.4% of the time. The presence radiates from cell H to the right, with decreasing observations: 55.2% in cell G, 13.8% in cell F, and 0% in cell E. Superiorly (cranially) and inferiorly (caudally) to cell H, the presence of the stomach also diminishes, with 58.6% in cell D and 48.3% in cell L. On average, the inferior margin of the stomach was found 34.18 ± 14.44 mm (95% CI: 22.11–46.25 mm) inferior to the costal border within the

mid-sagittal plane. Within the left midclavicular line, the inferior margin of the stomach was found on average to be 19.51 ± 11.13 mm (95% CI: 14.81–24.21 mm) inferior to the costal margin. On one occasion, the stomach was observed within the right midclavicular line, and the inferior margin of the stomach was found 19.11 mm inferior to the costal border.

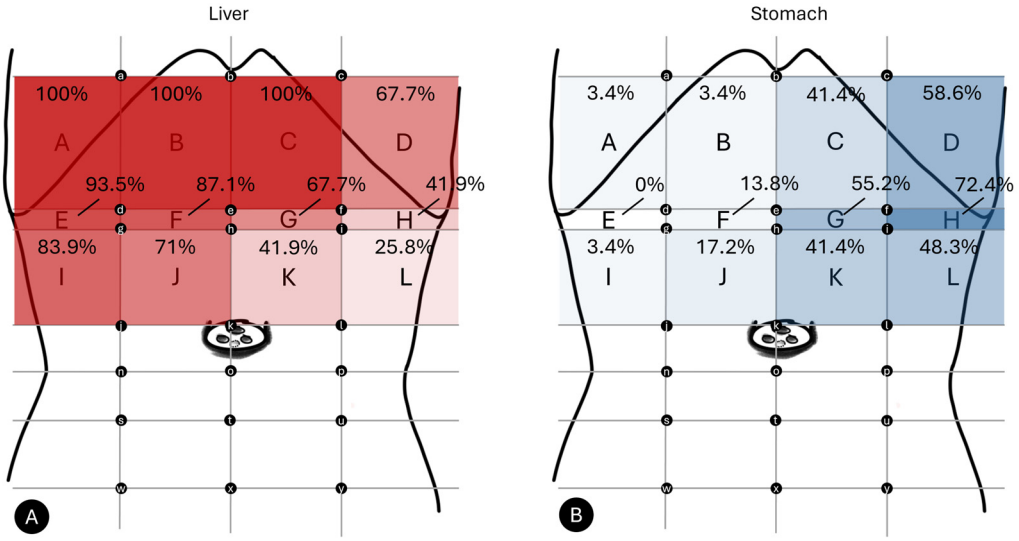


Figure 4. Visual representation of the liver (**A**) and stomach (**B**) frequency (if present, entirely or partially) within the related anatomical cells. Darker shades represent cells that occupy the organ more often. In contrast, lighter shades indicate that the organ was found less frequently in the specific cell.

3.4. Inter-Observer and Intra-Observer Error Analysis

The intra-observer error analysis indicated no significant difference between the principal investigator's initial observations and those made to test repeatability ($p > 0.05$). The intra-observer error analysis also showed no biases in the measured variables. The inter-observer error analysis of accuracy revealed some bias in the measurement ($p < 0.05$). As such, individual analysis of the measurement pairs was conducted and indicated bias at point "p" (1.16 ± 1.27 mm; $p = 0.01$), at the intersection of the left midclavicular line and the horizontal line through McBurney's point for measurements made for the deep vascular structures of the anterior abdominal wall. The second observer's measurements were consistently above those made by the principal investigator, with the 95% CI of the difference ranging from −0.21 mm to −0.06 mm, with a mean difference of −0.14 mm. These differences do not invalidate the topographical measurements, but highlight the narrow tolerances when referring to a typical trocar placement and diameter. Moreover, when comparing the internal vasculature and organ measurements of the co-author and the principal investigator, numerous measurement biases were observed between the pair ($p < 0.05$). The difference between the pair was 1.67 mm at point "I" medially towards the umbilical vein (20.97 ± 6.39 mm), a difference of 1.16 mm at point "u" medially (9.44 ± 3.61 mm), and a difference of 1.37 mm was observed from the costal border to the inferior margin of the liver (17.34 ± 8.24 mm). All these differences could be considered as small and less significant when considering the overall measurement. However, all three measurements the co-author obtained had a value smaller than the principal investigator's original measurements. Although there is a strong bias, the authors determined that the differences are not significant, given the proximity to the zero value. It should be noted that this assessment was conducted on a small subset of the overall experimental group ($n = 5$, about 16% of the 30 total specimens). While this subsample is adequate for detecting major

systematic biases or significant methodological issues, the limited sample size naturally reduces the statistical power needed to define very precise confidence limits of agreement.

4. Discussion

Within this current study investigating low-birth-weight neonatal anatomy, a reduced vascular midline corridor was observed, exhibiting greater distances to the nearest deep vasculature compared to their lateral counterparts along the midclavicular lines. For instance, the minimum circumferential distance from deep vessels at midline points "e", "h", and "o" averaged 6.84 mm, 6.88 mm, and 6.66 mm, respectively. In contrast, the distances at lateral points at the level or inferior to the umbilicus, such as "j", "l", "n", and "p, were, on average, smaller at 1.08 mm, 1.45 mm, 1.75 mm, and 1.16 mm, respectively. At the level of the umbilicus, the closest deep vasculature is found 10.87 mm to the left and 9.70 mm to the right of the midline. Even more caudally, the closest deep vasculature at the level of McBurney's point was 9.49 mm to the left and 9.90 mm to the right.

The superior and inferior epigastric arteries have been shown to exhibit considerable variation in their branching patterns and intramuscular course [5,6,16]. This demonstrates inherent anatomical variability in both its vascular and neural structures, while the iliohypogastric and ilioinguinal nerves may also vary in their course relative to commonly used surface landmarks [17]. Although the present study demonstrates consistent spatial trends, including a relative reduction in vascular density along the midline, these findings should be interpreted as probabilistic rather than absolute.

From a clinical perspective, bleeding from trocar or port sites from superficial vessels is often easily controlled with localised pressure, whereas injury to the deep vascular system can lead to haematomas or intra-abdominal bleeding which is typically more difficult to manage [18]. Epstein and Ellis [19], as well as Rao et al. [20], studied the course of the inferior epigastric artery in adults. They found that the branches of the inferior epigastric artery are highly variable, but found that within the midline of the abdomen, the presence of vasculature was reduced, and that the main stem of the inferior epigastric artery can be avoided if a trocar is placed lateral to the point defined by the distance two-thirds from the ASIS towards the midline within a horizontal plane [19,20]. This study found the same high variability and a reduced vascular midline within this low-birth-weight neonatal sample, as previously reported by Epstein and Ellis [19] and Rao et al. [20]. The minimal distances to deep vessels along the midclavicular lines ranged between 3.10 mm and 6.63 mm medially and 2.08 mm and 5.51 mm laterally, and the minimal distance to superficial vessels along the midclavicular lines ranged between 3.11 mm and 4.58 mm medially and 1.97 mm and 4.83 mm laterally. This quantification of vascular relations provides anatomical evidence to support that all secondary ports should be placed under direct laparoscopic visualisation to avoid injury to the superficial and inferior epigastric vessels.

The anatomical findings from this study lend themselves to translation into clinical practice, helping clinicians reconsider laparoscopic port placement approaches. When considering a supra-umbilical working port placement after successful insufflation for procedures in the upper abdomen, such as a Nissen fundoplication or cholecystectomy, both the location of the vasculature and viscera should be considered. Considering the neonatal liver and the location of the stomach, as this study found, they extend below the costal margin, averaging 17.34 mm at the right midclavicular line, 20.61 mm in the midline, and 12.41 mm at the left midclavicular line. The stomach was also frequently present in the upper left abdominal quadrant (i.e., cell H). This demonstrates that an optimal port strategy cannot be based solely on vascular anatomy; it requires an integrated understanding of both vascular and visceral topography to ensure both safety and adequate surgical access for the chosen procedure. The results from this study support a 5 mm working port placed at or

near Lee-Huang's point ('h') [2]; a 3 mm or 5 mm left-hand working port in the subcostal region, just left of the midline (near 'e') [21]; a 3 mm or 5 mm right-hand working port along the right midclavicular line, placed caudally to the inferior margin of the liver (near 'g'); and a 3 mm subxiphoid port (near 'b') [2]. This configuration prioritises the safety of the midline corridor for these port placements, respecting the position of the liver while accommodating a wide angle for working ports (Table 8, Figure 5). This configuration does not, however, consider the location of the umbilical vein, which in this study was found above the umbilicus within the midline of the abdomen.

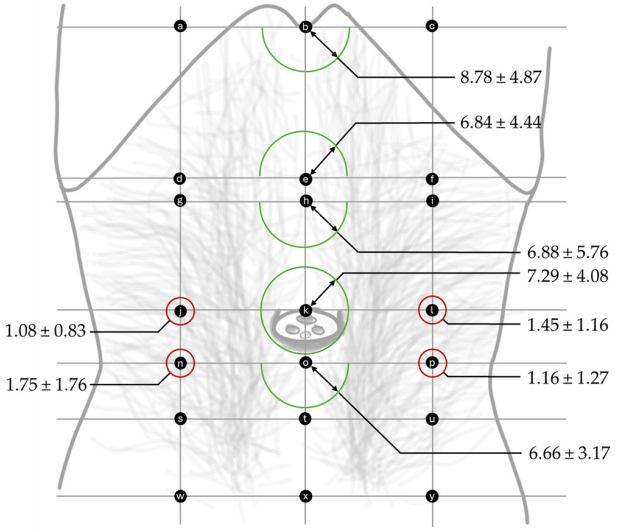


Figure 5. Mean circumferential distances (in mm) to deep vasculature from key anatomical landmarks.

Table 8. Mean circumferential distances to deep vasculature from key anatomical landmarks together with the percentile-based minimum distances to the deep vasculature.

Anatomical Landmark	Mean Circumferential Distance to Deep Vasculature (mm)	10th Percentile Distance (mm)	5th Percentile Distance (mm)
Point "b" (Midline, subxiphoid)	8.78 ± 4.87 mm (95% CI: 6.90–10.67 mm)	2.54	0.77
Point "e" (Midline, midway between xiphoid and umbilicus)	6.84 ± 4.44 mm (95% CI: 5.21–8.47 mm)	1.15	0.00 *
Point "h" (Lee-Huang's point)	6.88 ± 5.76 mm (95% CI: 4.73–9.03 mm)	0.00 *	0.00 *
Point "j" (Right midclavicular, transumbilical)	1.08 ± 0.83 mm (95% CI: 0.77–1.39 mm)	0.02	0.00 *
Point "k" (Umbilicus)	7.29 ± 4.08 mm (95% CI: 5.79–8.78 mm)	2.06	0.58
Point "l" (Left midclavicular, transumbilical)	1.45 ± 1.16 mm (95% CI: 1.02–1.88 mm)	0.00 *	0.00 *
Point "n" (Right midclavicular line, lower quadrant)	1.75 ± 1.76 mm; (95%CI: 1.11–2.40 mm)	0.00 *	0.00 *
Point "o" (Midline, at the horizontal line through McBurney's point)	6.66 ± 3.17 mm (95%CI: 5.49–7.82 mm)	2.60	1.45
Point "p" (Left midclavicular, lower quadrant)	1.16 ± 1.27 mm (95%CI: 0.68–1.64 mm)	0.00 *	0.00 *

* Physical distances to deep vasculature cannot be less than zero. Although raw calculations may produce negative values, these are limited to 0.00 since physically, negative distances are impossible.

While mean distances provide a useful overview of spatial relationships, they may underestimate the proximity of vascular structures. To provide a more conservative, clinically relevant interpretation, 5th- and 10th-percentile distances were calculated to represent the minimum expected distance to vascular structures for the majority of the population. These percentile values highlight the potential for small safety margins, even in regions that appear relatively less vascular when considering mean values alone, and support the need for cautious port placement and the use of direct visualisation where possible (Table 8).

The umbilicus (point "k") presents as an anatomical challenge. The current study's data on superficial vasculature indicate a relatively vessel-free zone around the umbilicus (mean distances of 7.80–11.20 mm). However, surgeons need to consider the deeper-lying umbilical vein, superiorly, and the umbilical arteries and urachus, inferiorly, within the neonatal population. This anatomical relationship provides a strong rationale for the common clinical preference for the open (Hasson) technique over a blind Veress needle insertion for primary umbilical access. Clinical studies have reported a very low incidence of clinically significant embolism [22]. The primary danger at this site is not superficial but deep, and not from the inherent properties of CO_2 insufflation but from procedural technique in the context of patent umbilical vessels. An air embolism can occur if insufflation tubing is not purged correctly [22].

Placement of a primary camera port is primarily achieved through the umbilicus, or just inferior to the umbilicus, within the infraumbilical fold [2]. A primary camera port at the umbilicus ('k') can provide a sufficient panoramic view, but should be placed using an open technique to avoid umbilical vessel injury [2]. This study demonstrated that within this neonatal sample, the closest deep vascular structure to the left of the umbilicus was 10.87 ± 4.40 mm, and 3.08 ± 2.74 mm to the right. Considering the superficial and deep vasculature in this sample, a primary camera port placed lateral to the umbilicus, preferably to the left, would be considered a safe anatomical location to penetrate the abdomen either through an open or blind access. When the primary camera port via umbilical access is contraindicated, surgeons may consider alternative entry sites, such as Palmer's point in the left upper quadrant. While a standard alternative in adults, its use in neonates warrants extreme caution. The adult landmark, typically 3 cm below the costal margin within the left midclavicular line, is where the liver is protected by the rib cage [23].

The findings of increased lateral vasculature in neonates align with advanced imaging studies performed in adults by Bowness et al. [24] and Le Saint-Grant et al. [25]. They demonstrated through computed tomography and ultrasound evaluation that the safest site to penetrate the rectus abdominis muscles, with respect to avoiding the inferior epigastric arteries, is at the transpyloric plane, while regions near the anterior superior iliac spines show a high vascular presence [24,25]. The perforator vessels [5,16,26] highlight the variable intramuscular paths that supply the skin. Kostov [6] underscores that a failure to appreciate this vascular anatomy during abdominal incisions leads to complications [6]. While their results were established in adult reconstructive and general surgery, this study's data echoes the same hazardous lateral vascular density in the neonatal abdomen. Fixed anatomical landmarks cannot consistently predict the exact location of underlying vessels or nerves in every individual. This variability further supports the recommendation that lateral port placement should be performed under direct visualisation.

This current neonatal study suggests the liver extends significantly below the costal margin, in the left midclavicular line, with the stomach also frequently occupying this region, cautioning the use of a blind Veress needle insertion below the costal margin. As such, the neonatal equivalent of Palmer's point, from the anatomical findings from this sample, suggests a blind Veress needle insertion, where the liver and stomach would not

be in danger, should be significantly below the costal margin in the left midclavicular line, considering the upper limit of the 95% CI for the stomach. The baseline measurements were obtained on non-distended, flaccid abdominal walls. The induction of pneumoperitoneum in a live patient dynamically alters parietal-visceral spatial relationships. Therefore, these static cadaveric thresholds must undergo clinical validation before they can be reliably implemented in routine clinical practice. The contralateral equivalent of Palmer's point below the costal margin within the right midclavicular line would suggest a blind Veress needle below 20.42 mm would avoid the liver, as per the upper limit of the 95% CI. As a blind insertion of a Veress needle carries a high risk of direct perforation of the liver or stomach, this study recommends that entry at this site be performed using an open technique.

Procedures below the umbilicus, within the lower abdomen and pelvis, such as appendicectomy or colectomy, require a different strategy. From this study, points 'n' and 'p', which have minimal vascular distances of approximately 1–2 mm, indicate that secondary working ports should be placed under direct visualisation, lateral to the rectus sheath, to avoid the inferior epigastric vessels. This aligns with existing descriptions of paediatric appendicectomy port placement while providing the quantitative anatomical justification for the techniques used [27]. This study provides surgeons with anatomical data to consider alternative positioning of the secondary port without compromising patient safety.

4.1. Limitations of the Study

The use of formalin-fixed body donations, while necessary for detailed dissection, introduces inherent limitations related to altered tissue properties and the absence of physiological factors such as blood pressure and muscle tone. Fixation reduces tissue elasticity and may result in some degree of dimensional change, potentially altering the spatial relationships observed from those in living tissue. Furthermore, the dissections were performed on a flaccid abdominal wall, without the distension created by pneumoperitoneum during live surgery. This insufflation-induced expansion increases the distance between the abdominal wall and underlying viscera and may alter the spatial relationships observed. These factors should be considered when translating the present findings to clinical practice.

The exact gestational ages were not available for this very-low- to low-birth-weight group. Therefore, the quantitative results should be interpreted with caution when applying them to full-term, normal-weight neonates. The sample consisted predominantly of Black South African neonatal body donations (86.7%), which, while appropriate for a descriptive anatomical study, may not capture the full spectrum of anatomical variation present in the broader neonatal population. Additionally, the mean weight of the sample (1.77 ± 1.16 kg) is less than that of typical full-term neonates, and this should be considered when interpreting the findings.

The small amount of subcutaneous fat and the notably large liver size significantly alter the distance from the epidermis to deep blood vessels compared to full-term, normal-weight infants. Performing statistically valid stratified correlation analyses based on weight, crown-heel length, or precise gestational age was not feasible, as the resulting subgroups lacked enough power for reliable conclusions. Therefore, the quantitative maps from this study should be applied with caution to full-term or demographically different neonatal groups. While there is no definitive evidence to suggest clinically significant differences in the course of the anterior abdominal wall vasculature between different population groups, the findings should be validated in more diverse populations to ensure their global applicability.

Finally, multiple directional and circumferential measurements were obtained from a geometric grid applied to each specimen, resulting in a dataset that exhibits intra-class correlation, also known as spatial clustering. A single neonatal specimen with a complex, dense, or unusual bilateral vascular branching provides multiple data points that can influence the overall analysis, potentially giving a false impression of localised density variations across nearby grid cells. Although pooling data in this way is acceptable for descriptive anatomical purposes, the non-independent nature of these data points means that the variances and standard deviations should be viewed as topographical patterns rather than precise biological probabilities.

4.2. Future Research Directions

In vivo validation of this cadaveric data with the use of non-invasive imaging techniques, such as high-frequency ultrasonography with Doppler mapping, could also be used to prospectively map the course of the inferior epigastric vessels in live neonates prior to surgery, allowing for a direct comparison with our anatomical findings. Finally, this data could form the basis for developing advanced surgical planning technologies, such as preoperative planning software or augmented reality systems that could overlay these anatomically based measurements onto the patient's abdomen, guiding surgeons to the optimal port sites with precision.

5. Conclusions

This study provides a quantitative anatomical description of the anterior abdominal wall vasculature in very-low- to low-birth-weight neonates, demonstrating a zone of relatively reduced vasculature within the midline corridor and comparatively condensed lateral vascular regions. These findings support a port placement strategy that prioritises the midline where appropriate and emphasises the use of direct visualisation for lateral access. These findings provide an anatomical framework for surgeons to optimise their technique for both supraumbilical and infraumbilical procedures and a rationale for placing a primary camera port lateral to the umbilicus. Ultimately, this study contributes to the ongoing refinement of neonatal minimal access surgeries.

Author Contributions: D.J.v.T.: Conceptualisation, Methodology, Formal analysis, Investigation, Writing—Original Draft, Visualisation. N.K.: Methodology, Validation, Writing—Review and Editing, Supervision. M.L.v.N.: Conceptualisation, Clinical contextualisation, Validation, Writing—Review and Editing. A.v.S.: Conceptualisation, Resources, Writing—Review and Editing, Project administration, Supervision. All authors have read and agreed to the published version of the manuscript.

Funding: This work is based on the research supported by the National Research Foundation (NRF) of South Africa (grant number: 120410). The funding source had no involvement in the study design, data collection, analysis, and interpretation of the data; in the writing of the report; or in the decision to submit the article for publication.

Institutional Review Board Statement: The study adhered to the South Africa National Health Act of 2003, the Declaration of Helsinki (2024), and did not collect any identifiable information, as approved by the Research Ethics Committee (ethics reference no: 224/2023) on 2023-07-12 at the Faculty of Health Sciences, University of Pretoria.

Informed Consent Statement: The prosection was conducted on a bequeathed embalmed human neonatal cadaver, acquired through either a family donation or as an unclaimed body, forming part of the Department of Anatomy's cadaver collection. In compliance with the National Health Act, 61 of 2003, and in adherence to the ethical guidelines of the Declaration of Helsinki (2024), no identifiable information was collected, ensuring consistency, integrity, and quality throughout the research.

Data Availability Statement: The original contributions presented in this study are included in the article. Further inquiries can be directed to the corresponding author.

Acknowledgments: The authors sincerely thank those who donated their bodies to science, allowing anatomical research to be performed. Results from such research can potentially enhance overall knowledge, leading to improvements in patient care. Therefore, these donors and their families deserve our highest gratitude. Additionally, the authors express their gratitude towards the medical personnel at Steve Biko Academic Hospital for their valuable contributions in scanning the body donations. Moreover, the authors extend their gratitude to Hounsh Munshi for her insights and assistance with generating Bland–Altman plots. Furthermore, the authors wish to express their appreciation to Jade Sterling and Michelle Cremer for their invaluable assistance with language and grammar editing. During the drafting process, the authors utilised certain functionalities of Gemini (version 2.5 Pro, Google, 2025), including its "Deep Research" feature, to collect relevant research articles. They also employed Grammarly (version 1.2.167.1681, Grammarly, 2025) for rephrasing and clarification, alongside basic grammar and spelling checks. After utilising these tools, the authors carefully reviewed and edited the content as necessary, ultimately taking full responsibility for the published material.

Conflicts of Interest: The authors declare that there are no conflicts of interest regarding the publication of this paper.

Abbreviations

The following abbreviations are used in this manuscript:

ASIS	Anterior Superior Iliac Spine
CI	Confidence Interval
CO2	Carbon dioxide
SD	Standard Deviation
Sup	Superior
Inf	Inferior
Med	Medial
Lat	Lateral

References

1. Davenport, M. Laparoscopic surgery in children. *Ann. R. Coll. Surg. Engl.* **2003**, *85*, 324. [CrossRef]
2. Holcomb, G.W.; Rothenberg, S.S. Principles of Laparoscopic Surgery. In *Atlas of Pediatric Laparoscopy and Thoracoscopy*, 2nd ed.; Holcomb, G.W., III, Rothenberg, S.S., Eds.; Elsevier: Amsterdam, The Netherlands, 2021; pp. 3–8.
3. Gans, S.L.; Berci, G. Advances in endoscopy of infants and children. *J. Pediatr. Surg.* **1971**, *6*, 199–233. [CrossRef]
4. Jelinek, L.A.; Scharbach, S.; Kashyap, S.; Ferguson, T. Anatomy, Abdomen and Pelvis: Anterolateral Abdominal Wall Fascia. In *StatPearls*; StatPearls Publishing: Treasure Island, FL, USA, 2026. Available online: https://www.ncbi.nlm.nih.gov/books/NBK459392/ (accessed on 24 March 2026).
5. Rozen, W.M.; Ashton, M.W.; Taylor, G.I. Reviewing the vascular supply of the anterior abdominal wall: Redefining anatomy for increasingly refined surgery. *Clin. Anat.* **2008**, *21*, 89–98. [CrossRef]
6. Kostov, S.; Dineva, S.; Kornovski, Y.; Slavchev, S.; Ivanova, Y.; Yordanov, A. Vascular Anatomy and Variations of the Anterior Abdominal Wall—Significance in Abdominal Surgery. *Prague Med. Rep.* **2023**, *124*, 108–142. [CrossRef]
7. Park, S.O.; Imanishi, N.; Chang, H. The Anatomic Features and Role of Superficial Inferior Epigastric Vein in Abdominal Flap. *Arch. Plast. Surg.* **2022**, *49*, 482–487. [CrossRef] [PubMed]
8. Vasquez, J.M.; Demarque, A.M.; Diamond, M.P. Vascular complications of laparoscopic surgery. *J. Am. Assoc. Gynecol. Laparosc.* **1994**, *1*, 163–167. [CrossRef]
9. Schaverien, M.; Saint-Cyr, M. Arterial and Venous Anatomies of the Deep Inferior Epigastric Artery Perforator and Superficial Inferior Epigastric Flaps. *Plast. Reconstr. Surg.* **2010**, *125*, 1045–1046. [CrossRef]
10. Hurd, W.W.; Amesse, L.S.; Gruber, J.S.; Horowitz, G.M.; Cha, G.M.; Hurteau, J.A. Visualization of the epigastric vessels and bladder before laparoscopic trocar placement. *Fertil. Steril.* **2003**, *80*, 209–212. [CrossRef]
11. Pickett, S.D.; Rodewald, K.J.; Billow, M.R.; Giannios, N.M.; Hurd, W.W. Avoiding Major Vessel Injury During Laparoscopic Instrument Insertion. *Obstet. Gynecol. Clin. N. Am.* **2010**, *37*, 387–397. [CrossRef] [PubMed]

12. Brusciano, V.; Lecce, M. Advantages of the use of ultrasound in newborn vascular access: A systematic review. *J. Ultrasound* **2024**, *27*, 203–207. [CrossRef] [PubMed]
13. Schindelin, J.; Arganda-Carreras, I.; Frise, E.; Kaynig, V.; Longair, M.; Pietzsch, T.; Preibisch, S.; Rueden, C.; Saalfeld, S.; Schmid, B.; et al. Fiji: An open-source platform for biological-image analysis. *Nat. Methods* **2012**, *9*, 676–682. [CrossRef] [PubMed]
14. Węglarczyk, S. Kernel density estimation and its application. *ITM Web Conf.* **2018**, *23*, 00037. [CrossRef]
15. Bland, J.M.; Altman, D.G. Statistical methods for assessing agreement between two methods of clinical measurement. *Int. J. Nurs. Stud.* **2010**, *47*, 931–936. [CrossRef]
16. van Tonder, D.J.; Keough, N.; van Niekerk, M.L.; van Schoor, A. Variant Superficial Epigastric Supply to the Anterior Abdominal Wall Arising from Inferior Epigastric Perforators: A Neonatal Case Report. *Anatomia* **2026**, *5*, 7. [CrossRef]
17. Manolakos, K.; Zygogiannis, K.; Manolakos, O.; Mousa, C.; Papadimitriou, G.; Fotoniatas, I. Anatomical variations of ilioinguinal nerve: A systematic review of the literature. *Surg. Neurol. Int.* **2024**, *15*, 225. [CrossRef]
18. Deziel, D.J. Trocar- and Port-Related Bleeding. In *The Sages Manual*; Springer: New York, NY, USA, 2006; pp. 254–262. [CrossRef]
19. Epstein, J.; Arora, A.; Ellis, H. Surface anatomy of the inferior epigastric artery in relation to laparoscopic injury. *Clin. Anat.* **2004**, *17*, 400–408. [CrossRef]
20. Rao, M.; Swamy, V.; Arole, V.; Mishra, P. Study of the course of inferior epigastric artery with reference to laparoscopic portal. *J. Minim. Access Surg.* **2013**, *9*, 154–158. [CrossRef]
21. Holcomb, G.W.; van der Zee, D.C. Laparoscopic Fundoplication. In *Atlas of Pediatric Laparoscopy and Thoracoscopy*, 2nd ed.; Holcomb, G.W., III, Rothenberg, S.S., Eds.; Elsevier: Amsterdam, The Netherlands, 2021; pp. 11–20.
22. Patterson, K.N.; Beyene, T.J.; Minneci, P.C.; Diefenbach, K.A. Rates of Air Embolism in Pediatric Patients Undergoing Surgical Procedures of the Peritoneum. *J. Laparoendosc. Adv. Surg. Technol.* **2022**, *32*, 1220–1227. [CrossRef] [PubMed]
23. Palmer, R. Safety in laparoscopy. *J. Reprod. Med.* **1974**, *13*, 1–5. [PubMed]
24. Bowness, J.; Seeley, J.; Varsou, O.; McKinnie, A.; Zealley, I.; McLeod, G.; Grant, C. Arterial Anatomy of the Anterior Abdominal Wall: Evidence-Based Safe Sites for Instrumentation Based on Radiological Analysis of 100 Patients. *Clin. Anat.* **2020**, *33*, 350–354. [CrossRef]
25. Le Saint-Grant, A.; Taylor, A.; Varsou, O.; Grant, C.; Cezayirli, E.; Bowness, J. Arterial anatomy of the anterior abdominal wall: Ultrasound evaluation as a real-time guide to percutaneous instrumentation. *Clin. Anat.* **2021**, *34*, 5–10. [CrossRef] [PubMed]
26. Meyerov, J.; Ram, R.; Grinsell, D. Refining the abdominal wall perforasome with clinical application. *J. Plast. Reconstr. Aesthetic Surg.* **2025**, *105*, 283–291. [CrossRef] [PubMed]
27. Gibbons, A.T.; Lai, S.W.; Ponsky, T.A. Laparoscopic Appendectomy. In *Atlas of Pediatric Laparoscopy and Thoracoscopy*, 2nd ed.; Holcomb, G.W., III, Rothenberg, S.S., Eds.; Elsevier: Amsterdam, The Netherlands, 2021; pp. 63–69.

Disclaimer/Publisher's Note: The statements, opinions and data contained in all publications are solely those of the individual author(s) and contributor(s) and not of MDPI and/or the editor(s). MDPI and/or the editor(s) disclaim responsibility for any injury to people or property resulting from any ideas, methods, instructions or products referred to in the content.